J Therm Anal Calorim (2016) 126:1567–1577
DOI 10.1007/s10973-016-5650-0

Synthesis, characterization and thermal stability of cobalt salts of Keggin-type heteropolyacids supported on mesoporous silica

Alexandru Popa[1] · Viorel Sasca[1] · Danica Bajuk-Bogdanović[2] · Ivanka Holclajtner-Antunović[2]

Received: 19 January 2016 / Accepted: 16 June 2016 / Published online: 30 June 2016

Abstract Some heteropoly salts–mesoporous silica composites were prepared from Co salt of molybdophosphoric acid $CoHPMo_{12}O_{40}$ (CoHPM) by supporting on mesoporous silica in different concentrations (20–40 mass% CoHPM) of active phase. The structure and texture of these CoHPM/silica composites were studied by powder X-ray diffraction, Fourier transformed infra-red (FT-IR) and micro-Raman spectroscopy, nitrogen physisorption at 77 K and scanning electron microscopy with energy-dispersive X-ray spectroscopy (SEM–EDS). Thermal stability was investigated by thermogravimetric analysis, differential thermal analysis and differential scanning calorimetry. FT-IR and Raman studies showed that heteropoly anions preserved their Keggin structure after impregnation on mesoporous silica support. From SEM–EDS analysis, it observed that for low loading of active phase, the average content of chemical elements (Mo, P and Co) is close to the stoichiometric values, while for higher loadings, the samples exhibit some deviation of concentration values from the stoichiometric ones. The mesoporous silica–HPA composites are thermally more stable than the parent acids, due to the strong anion-support interaction.

Keywords Cobalt phosphomolybdate · Mesoporous silica · Tween 60 · Raman spectroscopy · Thermogravimetric analysis

✉ Alexandru Popa
alpopa_tim2003@yahoo.com

[1] Institute of Chemistry Timişoara, Bl.Mihai Viteazul 24, 300223 Timisoara, Romania

[2] Faculty of Physical Chemistry, University of Belgrade, P.O. Box 47, Belgrade 11158, Serbia

Introduction

The study of the chemistry and reactivity of early transition metal–oxygen–anion clusters (more generally referred to as polyoxoanions or polyoxometalates) has been growing continuously in recent decades. Polyoxometalates (POMs) have unique physical and chemical properties, e.g., strong Brønsted acidity, strong oxidizing capacity with application in photochemistry, different fields of medicine (in anti-HIV chemotherapy) and as green catalysts and efficient adsorbents. Owing to their versatility in composition and chemical–physical features, *multifunctional POM materials could be designed for different environmental applications*, such as toxic gas sequestration, wastewater decontamination, fine chemical production, corrosion and radioactive waste processing. [1, 2].

The following POMs anions: $PMo_{12}O_{40}^{3-}$, $PW_{12}O_{40}^{3-}$, $SiMo_{12}O_{40}^{4-}$, $SiW_{12}O_{40}^{4-}$, $CoW_{12}O_{40}^{6-}$ and $PMo_{11}VO_{40}^{3-}$, could be used as efficient wet chemical adsorbents to extract CO_2 from flue gas according to a recent patent [3]. Jiang et al. *have reported the preparation* via *sol–gel technique* of a zirconia-supported heteropolyacid (HPA), $H_3PW_{12}O_{40}/ZrO_2$, which contains both Brønsted and Lewis acid sites. These composites were effective catalysts for selective synthesis of dimethyl carbonate (DMC) from methanol and CO_2. The effects such as the amount of catalysts, reaction temperature and CO_2 pressure on the DMC formation were studied, indicating that the catalytic activity depends strongly on the CO_2 pressure [4].

Pure HPAs generally show low catalytic reactivity owing to their small surface area. In order to be more effective for catalytic reactions, HPAs are usually impregnated or incorporated on suitable porous materials with high surface area and/or by replacement of protons with different cations. A lot of matrices have been used to

support HPAs and *their salts in order to attain better accessibility of reactants to the catalysts active sites*. Among the supports that have been mentioned in different studies are: mesoporous silica [5–7], titania [8, 9], active carbon [10, 11], salts of heteropolyacids [12–14], polymeric materials [15, 16] and different molecular sieves: MCM-41, SBA-15, SBA-3, HMS [17–26].

Owing to their strong acidity, HPAs of Keggin structure like $H_3PW_{12}O_{40}$ (HPW), $H_3PMo_{12}O_{40}$ (HPM) and their acidic salts are highly active for various kinds of acid-catalyzed reactions [27–29]. The H^+ protons which are known to be responsible for acid-catalysed reactions can be completely or partially exchanged, with different cations without affecting the primary Keggin structure. Partial substitution of protons by these cations may result in changes of the number of available surface acidic sites [30, 31].

The synthesis of ordered mesoporous silica materials can be performed using various cationic and non-ionic surfactants and silica sources. Toufaily et al. [32] used different types of non-ionic and ionic surfactants. These materials exhibit structures with uniform channel diameters over a range comparable with the MCM-41 type materials. They prepared a solid catalyst by direct incorporation of HPW into organized mesoporous silica. The structure of inorganic species was controlled either by a mixture of non-ionic and cationic surfactant or only by a non-ionic one.

In a previous work, we studied the direct incorporation of $H_3PMo_{12}O_{40}$ and $H_4PVMo_{11}O_{40}$ into mesoporous silica during the synthesis [7]. The synthesis of mesoporous silica containing HPAs was carried out in acidic media by using a mixture of cationic and non-ionic surfactants, such as cetyltrimethylammonium bromide (C_{16}TMABr) and Triton (TX-100) or Tween 100. In the study, a comparison between direct incorporation of HPAs into mesoporous silica and impregnation of HPAs on mesoporous silica was done. After incorporation or impregnation, the HPAs anions preserved their Keggin structure on the surface of mesoporous silica–heteropolyacid composites and form finely dispersed HPAs species. The favourable effects of HPAs incorporation on mesoporous silica are the increasing of pore volume and specific surface area, which renders the silica–heteropolyacid composites appropriate for heterogeneous catalysis. The mesoporous silica–HPAs composites are thermally more stable than the parent acids, due to the strong anion-support interaction.

Although different HPAs salts (especially of $H_3PW_{12}O_{40}$ acid) based on only one type of cation or mixed salts have been extensively reported, the influence of surface coverage of Co salts of 12-molybdophosphoric supported on different supports in reference to the bulk solids has not been significantly explored in the literature.

The aim of this work was to synthesize and characterize the $CoHPMo_{12}O_{40}$-silica composites with different concentration of active phase and to investigate their thermal stability in reference to the corresponding bulk CoHPM. The synthesis of mesoporous silica was carried out in acidic media by using a non-ionic surfactant: Tween 60. In order to obtain highly dispersed heteropolyacid species, the Co salt of molybdophosphoric acid $Co_1HPMo_{12}O_{40}$ (CoHPM) was supported on mesoporous silica with Tween 60 in different concentration of active phase.

Materials and methods

Samples preparation

Molybdophosphoric acid, $H_3PMo_{12}O_{40}\cdot 12H_2O$, was purchased from Merck. The silicon source was tetraethoxysilane (TEOS) from Fluka. Polyethylene sorbitan-monostearate (Tween 60) from Merck was used as non-ionic surfactant. Sodium fluoride NaF, from Fluka, was employed as mineralizing agent.

The bulk CoHPM with Co/Keggin unit ratio of 1 was prepared by adding slowly drop wise the required amount of aqueous cobalt nitrate $Co(NO_3)_2$ to aqueous solution of HPM with vigorous stirring at room temperature. The precipitate obtained was aged in parent solution for 24 h at room temperature, followed by evaporation in vacuum at 323 K. For comparison, one group of samples was calcinated at 523 K for 4 h.

Organized mesoporous silica with Tween 60 was prepared by the hydrolysis of tetraethyl orthosilicate using non-ionic surfactants. The procedure was described in our previous work [7]. The synthesis was performed by sol–gel technique with the following molar composition: $1SiO_2$:0.067 Tween 60:0.04 NaF:148 H_2O. The solid product was filtered, washed with distilled water and dried in air for 6 h. Calcination for template surfactants removal was carried out under air by increasing temperature from 298 to 823 K with a rate of 2 °C/min and heating at 823 K for 4 h.

The mesoporous silica-supported HPAs were prepared by impregnation of active phase (CoHPM) on mesoporous silica with Tween 60 by two-step sequential impregnation method: first cobalt nitrate was impregnated by aqueous incipient wetness onto mesoporous silica with Tween 60, dried and calcined at 573 K and finally 12-molybdophosphoric acid was impregnated by a similar aqueous impregnation route. CoHPM is deposited by impregnation on the calcined samples of mesoporous silica with Tween 60 in the concentration loadings of 20, 30 and 40 mass%. The samples were denoted as 20, 30 and 40 CoHPM/Tween 60.

Samples characterization

The structure and texture of CoHPM impregnated on mesoporous silica were studied by PXRD, FT-IR and Raman spectrometry, low temperature nitrogen adsorption technique and scanning electron microscopy with energy-dispersive spectrometry (SEM–EDS). Thermal stability was investigated by thermogravimetric analysis (TG), differential thermal analysis (DTA) and differential scanning calorimetry (DSC).

Measurements of textural properties

Textural characteristics of the outgassed samples were obtained from nitrogen physisorption using a Quantachrome instrument, Nova 2000 series. The specific surface area S_{BET}, *average pore diameter* d_p and adsorption pore volume V_{pN2} were determined. Prior to the measurements, the samples were degassed to 10^{-5} Pa at 523 K. The BET specific surface area was calculated by using the standard Brunauer, Emmett and Teller method on the basis of the adsorption data. The pore size distributions were calculated applying the Barrett–Joyner–Halenda (BJH) method to the desorption branches of the isotherms. The IUPAC classification of pores and isotherms were used in this study.

Powder X-ray diffraction

Powder X-ray diffraction data were obtained with a XD 8 Advanced Bruker diffractometer using the Cu K_α radiation in the range $2\theta = 0.5°$–$5°$ at low angles and $2\theta = 5°$–$60°$. The scanning was made with a step size of 0.02° and a step time of 2 s.

Scanning electronic microscopy with energy-dispersive X-ray spectroscopy

Microstructure characterization of the catalyst particles was carried out with an energy-dispersive X-Max Large Area Analytical Silicon Drifted spectrometer (Oxford) coupled with scanning electron microscope JSM-6610 LV. The analyses were done under acceleration voltage of 15 kV, a beam current of 20 nA and a spot size of 1 μm. Appropriate internal and external standards were used for the analyses. Powder materials were deposited on adhesive tape fixed to specimen tabs and then ion sputter coated with gold.

Spectral characterization by Fourier transform infra-red and micro-Raman spectroscopy

The FT-IR absorption spectra were recorded with a Jasco 430 spectrometer (spectral range 4000–400 cm^{-1}, 256 scans, and resolution 2 cm^{-1}) using KBr pellets.

Micro-Raman spectra excited with a diode-pumped solid-state high-brightness laser (532 nm) were collected on a Thermo Scientific DXR Raman microscope, equipped with an Olympus optical microscope with infinity-corrected confocal optics, 25 μm pinhole aperture, standard working distance objective 50× and a CCD detector. The power of illumination at the sample surface was 0.5 mW. It is very important to record spectra with as low excitation laser power as possible to avoid destruction and/or changes of the sample due to the sample heating, especially in the analysis of molybdophosphates which are very thermally sensitive. The scattered light was analysed by the spectrograph with a grating of 1800 lines mm^{-1}. Acquisition time was 10 s with 10 scans. The laser spot diameter on the sample was 1 μm. Thermo Scientific OMNIC™ software was used for spectra collection and manipulation.

Thermal analysis

Thermal analysis was carried out using a *TG/DTA* 851-LF 1100 Mettler apparatus. The samples with mass of about 20 mg were placed in alumina crucible of 150 μl. The measurements were taken in dynamic air atmosphere with the flow rate of 50 mL min^{-1}, in the temperature range of 298–923 K with a heating rate of 10 K min^{-1} and an isothermal heating at 573 K for 60 min and at 923 K for 30 min.

DSC analysis was carried out with a Mettler Star system DSC 823 apparatus. The samples with mass of 20–40 mg were placed in Pt crucible of 150 μl. The measurements were taken in dynamic air atmosphere with the flow rate of 50 mL min^{-1}, in the temperature range of 303–923 K with a heating rate of 10 K min^{-1}.

Results and discussion

Porosity and surface area

All the N_2 adsorption–desorption isotherms of the parent mesoporous silica with Tween 60 and CoHPM impregnated on mesoporous silica show a typical adsorption curve of type IV (Fig. 1a–d). The specific surface area, pore volume and pore diameter determined from the isotherms using the BJH method are given in Table 1.

Isotherms of mesoporous silica with Tween 60 as a support and those impregnated with CoHPM show an obvious hysteresis loop at a relative pressure of $p/p_0 = 0.4$–0.8.

Pure CoHPM salt has low surface area and pore volume, textural characteristics which are increased by impregnation on mesoporous silica. However, samples of CoHPM salt impregnated on mesoporous silica with Tween

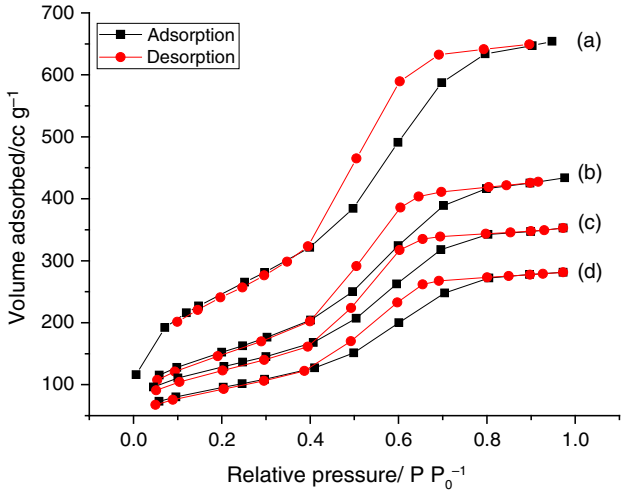

Fig. 1 Nitrogen adsorption–desorption plot of mesoporous silica with Tween 60 and CoHPM supported on Tween 60: mesoporous silica with Tween 60 (**a**) 20CoHPM/Tween60 (**b**), 30CoHPM/Tween60 (**c**), 40CoHPM/Tween60 (**d**)

60 have lower specific surface area and pore volume than pure silica (Table 1). The decrease of these characteristics is higher for higher amounts of impregnated CoHPM. This can be explained by the partial blockage of the mesopores of the support by HPAs particles. However, the pore size distribution curves with narrow pore size distribution within mesopore range with a maximum at about 37 Å are obtained for pure support and all composites (not shown).

PXRD analysis

The PXRD patterns at low angles for the initial mesoporous silica with Tween 60 show a single strong diffraction peak below 2.0° (2θ) (Fig. 2). The corresponding interplanar spacing d is about 62.7 Å. However, the appearance of a broad feature between 2 and 3° (2θ) can indicate the evolution of higher-order peak.

After the incorporation of CoHPM into the initial mesoporous silica framework, the d_{100} peak is slightly shifted to higher angles and broadened. This peak for 20, 30 and 40 CoHPM/Tween 60 composites is centred at 58.1, 58.9 and 59.7 Å, respectively. The intensity of this peak (typical for mesoporous materials) decreases with increasing amounts of the active phase, which indicates a pore-filling effect of the matrix.

XRD patterns at large angles (2θ = 5°–60°) of CoHPM/Tween 60 composites are similar to that of the support, without diffraction lines corresponding to HPA (not shown). This indicates that the CoHPM is highly dispersed at the molecular level in the silica matrix without phase segregation.

SEM-EDS characterization

Electron microscopic studies were performed for CoHPM–silica composites using SEM mode. The micrographs of samples 20CoHPM supported on silica, non-calcinated and calcinated at 527 K are displayed in Fig. 3a, b. The SEM image shows that CoHPM/Tween 60 composites are composed of spherical particles of CoHPM with an average diameter less than 1 μm and porous, irregularly shaped larger assembles, composed of primary silica particles matrix.

The chemical composition of silicon from support and of Mo, Co and P from active phase was obtained by EDS method. This method was acquired over a minimum of four areas of about 500 × 500 μm^2 on each sample. The analysis was repeated on different particles of the same batch in order to ensure the reproducibility of the obtained results.

Micro analytical data of EDS analysis show that the elements of active phase (cobalt, molybdenum and phosphorous) content distribution is relatively homogeneous and close to stoichiometric values.

For the uncalcined sample 20CoHPM/Tween 60 composites, the average content of Mo as mass% is close to the stoichiometric one: 12.78 is experimental value and stoichiometric value is 12.24 mass%. Also, P content (0.34 mass%) and Co content (0.59 mass%) are close to the stoichiometric values (Table 2). For all the composites, after calcination at 523 K, the content of Mo, Co and P are closer to stoichiometric values.

The mass ratios data for Co, P, and Mo related to Si in CoHPM–Tween 60 composites are summarized in Table 3. Comparing the experimental and stoichiometric values of Mo, P and Co concentration values, it can be observed that

Table 1 Textural properties of pure CoHPM and CoHPM/Tween 60 composites

Sample	Specific surface area/m^2 g^{-1}	Pore volume BJH_{Des}/cc g^{-1}	Average pore diameter BJH_{Des}/nm
CoHPM	*22.8*	*0.043*	*2.61*
20CoHPM/Tween 60	594.1	0.67	3.66
30CoHPM/Tween 60	451.6	0.55	3.63
40CoHPM/Tween 60	339.5	0.44	3.56
Mesoporous silica with Tween 60	878.0	1.01	3.67

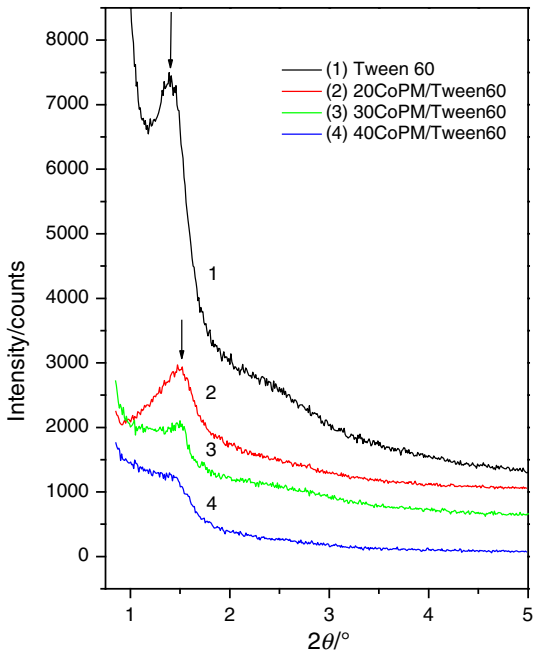

Fig. 2 X-ray diffraction pattern of CoHPM/Tween 60 composites

for higher loadings of active phase (30 and 40 %), the samples exhibit some small deviations, for both non-calcinated and calcinated ones. It could be supposed that active phase was less homogeneously dispersed inside the composites pores for higher than for low loadings of active phase.

In order to check the correctness of the values for Mo, P and Co composition, the composition values of the support as SiO_2 oxide were analysed. EDS analysis of uncalcined sample 20CoHPM/Tween 60 shows that the concentration of SiO_2 has a mean value of 79.3 (stoichiometric value is 80.0 mass%), while the calcined sample 20CoHPM/Tween 60 has a mean value of 80.4 (stoichiometric value is 80.0 mass%). *All these results show that calcination of samples has contributed to a better dispersion and more homogeneous distribution of active phase in the silica matrix*.

FTIR and micro-Raman spectrometry

Structural integrity of the Keggin anion in organized mesoporous silica with Tween 60–CoHPM composites was confirmed by FT-IR and micro-Raman spectroscopy. *The structure of Keggin ion* $PMo_{12}O_{40}^{3-}$ *consists of a* PO_4 *tetrahedron surrounded by four* Mo_3O_{13} *formed by edge-sharing octahedra*. These groups are connected with each other by corner-sharing oxygen. This structure gives rise to four types of oxygen, being responsible for the fingerprint bands of Keggin anion between 1200 and 700 cm^{-1}.

The Keggin structure of the bulk CoHPM is identified by characteristic IR spectrum with main vibrations at 1064, 966, 872, 785 cm^{-1} assigned to the stretching vibrations ν_{as} P–O_a, ν_{as} Mo=O_t, ν_{as} Mo–O_b–Mo and ν_{as} Mo–O_c–Mo [33, 34]. In addition, a broad, intense band centred around 3440 cm^{-1} (νO–H stretching) and a weak absorption at 1608 cm^{-1} (νH_2O bending) indicate the presence of water.

The introduction of heteropolyacids salts into the mesoporous silica matrix influenced the structure of resulted CoHPM/Tween 60 composites (Fig. 4). The characteristic bands are preserved, but they are broadened and partially overlapped by the strong absorption bands of silica (1090, 800 and 462 cm^{-1}). The vibration band at about 1090 cm^{-1} assigned to ν_{as}(Si–O–Si) is decreased to 1082 cm^{-1}; this strong and broad band completely overlaps a band assigned to the P–O asymmetric stretching vibration at 1064 cm^{-1}, while the band at 966 cm^{-1} in IR spectrum of pure CoHPM assigned to the ν_{as} Mo=O_t stretching vibration is shifted to 962 cm^{-1} in the spectrum of silica impregnated samples.

A band corresponding to the ν_{as} Mo–O_b–Mo vibration appears with moderate intensity at 875 cm^{-1} especially for higher loadings of CoHPM. The bands at 800 and 462 cm^{-1} can be assigned to ν_s (Si–O–Si) and δ (Si–O–Si) bonds, respectively [35]. In the spectra of mesoporous silica–CoHPM composites, the band of banding vibration is shifted to 1638 cm^{-1}. It is assigned to the H–O–H bending vibration of the free or adsorbed water molecules.

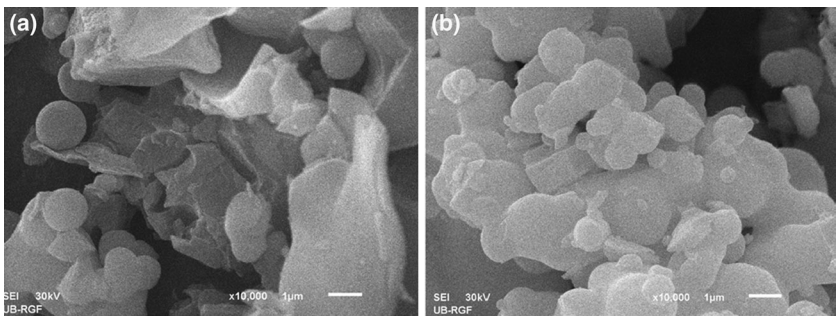

Fig. 3 SEM micrographs of **a** 20 CoHPM/Tween60 non-calcinated, **b** CoHPM/Tween60 calcinated at 523 K

Table 2 Energy dispersive X-ray (EDS) analysis data for Co, P and Mo in pure CoHPM and CoHPM/Tween 60 composites, initial solids and solids obtained after calcination at 523 K

Sample	Elemental analysis/mass%					
	Mo		P		Co	
	Exp.	Stoich.	Exp.	Stoich.	Exp.	Stoich.
CoHPM	*60.84*	*61.18*	*2.75*	*2.71*	*1.61*	*1.65*
20CoHPM/Tween 60	12.78	12.24	0.34	0.33	0.59	0.63
30CoHPM/Tween 60	18.26	18.35	0.57	0.49	0.85	0.94
40CoHPM/Tween 60	23.12	24.47	0.64	0.66	1.14	1.25
CoHPM_523 K	*61.03*	*61.18*	*2.72*	*2.71*	*1.63*	*1.65*
20CoHPM/Tween 60_523 K	12.10	12.24	0.35	0.33	0.63	0.63
30CoHPM/Tween 60_523 K	19.19	18.35	0.55	0.49	0.89	0.94
40CoHPM/Tween 60_523 K	23.79	24.47	0.55	0.66	1.15	1.25

Table 3 Mass ratios data for Co, P, Mo reported to Si in CoHPM/Tween 60 composites

	20CoHPM/Tween 60	30CoHPM/Tween 60	40CoHPM/Tween 60
Mo/Si	0.344	0.568	0.805
P/Si	0.009	0.018	0.022
Co/Si	0.016	0.026	0.039

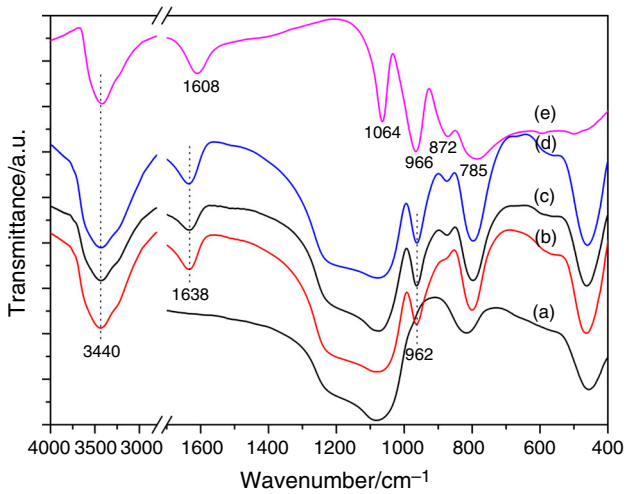

Fig. 4 FT-IR spectra of CoHPM/Tween 60 composites: mesoporous silica with Tween 60 (*a*) 20CoHPM/Tween60 (*b*), 30CoHPM/Tween60 (*c*), 40CoHPM/Tween60 (*d*), CoHPM (*e*)

Raman spectra of pure HPM, CoHPM and CoHPM/Tween 60 composites with various amounts of incorporated CoHPM are shown in Fig. 5. The Raman spectrum of bulk HPM (Fig. 5a) gives the main bands at 995, 976, 602 and 250 cm^{-1} assigned to symmetric (ν_s) and asymmetric (ν_{as}) vibrations of terminal oxygen ν_s (Mo–O_t) and ν_{as} (Mo–O_t), a combined stretching and bending motion of the Mo–O_b–Mo bonds of Mo_3O_{13} groups and symmetric stretch of P–O_a bonds [33, 34]. When protons are replaced by cation such as Co, the Raman spectrum is almost identical to that of parent acid with a slight shift of the main bands towards higher frequencies (Fig. 5b).

The Raman spectrum of mesoporous silica does not show vibration bands in this wavenumber region except strong fluorescence. So, the observed characteristic bands in the spectra of the studied composites originate only from CoHPM as the active phase.

Raman spectra of all investigated composites, before and after thermal treatment, show that mesoporous silica support does not induce destabilisation of CoHPM structure. In Raman spectra of CoHPM/Tween 60 composites, it could be observed a slight shift of the main bands towards lower frequencies related to pure CoHPM and parent acid HPM. The Keggin structure is preserved for all CoHPM contents, but the main characteristic features of the structure are observed at 991 cm^{-1} (ν_s Mo–O_t), 968 cm^{-1} (ν_{as} Mo–O_t), 596 cm^{-1} (ν_s Mo–O_c–Mo) and 243 cm^{-1} (ν_s Mo–O_a). The shift of the position of the main bands towards lower frequencies is a consequence of substrate interaction with the CoHPM. Due to this interaction, anion–anion interaction in the composites is decreased and the main peaks are red shifted [33].

After thermal treatment at 523 K, the Raman spectrum of CoHPM/Tween 60 composites shows only slight modifications. Raman spectra show that mesoporous silica support does not influence the structure of Keggin anion, it is still preserved. No characteristic bands of MoO_3 are

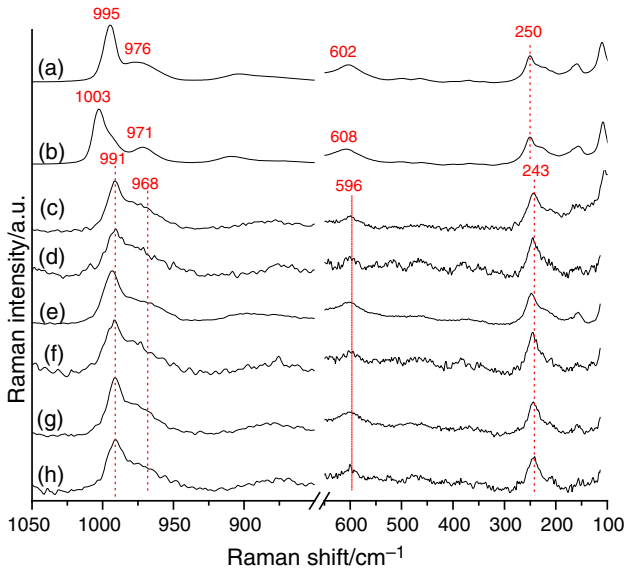

Fig. 5 Raman spectra of pure HPM, CoHPM and mesoporous silica with Tween 60–CoHPM composites: HPM (*a*) CoHPM calcinated at 523 K (*b*), 20CoHPM/Tween60 (*c*), 20CoHPM/Tween60 calcinated at 523 K (*d*), 30CoHPM/Tween60 (*e*), 30CoHPM/Tween60 calcinated at 523 K (*f*) 40CoHPM/Tween60 (*g*), 40CoHPM/Tween60 calcinated at 523 K (*h*)

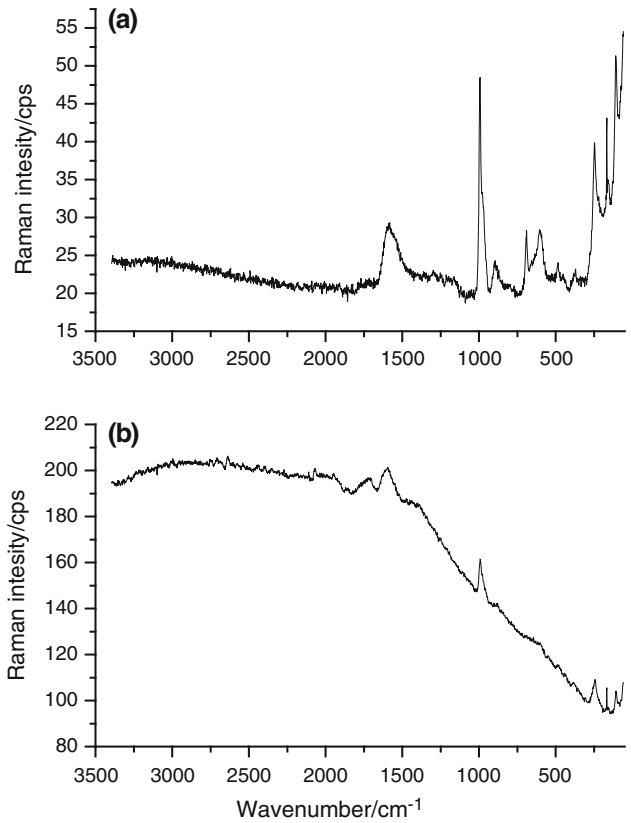

Fig. 6 Raman spectra of 40 CoHPM/Tween 60 composite before (**a**) and after calcination at 523 K (**b**)

detected as a result of Keggin structure collapse as observed by Yihang Guo et al. [36]. However, the original Raman spectrum (without baseline correction) of calcinated samples shows considerably stronger fluorescence than non-calcinated samples. The original Raman spectra of 40 CoHPM/Tween60 composite before and after calcination are presented in Fig. 6 as illustration. As substrate shows strong fluorescence in this wavenumber region, it is obvious that fluorescence from the substrate dominates in Raman spectrum of calcinated samples over the stretching of Keggin anion of active phase. It could be supposed that heat treatment causes better dispersion of active phase in mesoporous silica support which is in accordance with the literature [30].

Finally, it can be assumed that Raman spectroscopy confirmed that the Keggin structure is well preserved on the mesoporous silica support after its impregnation with CoHPM and that thermal treatment enabled better dispersion of the active phase in the support. This observation is in agreement with FT–IR results.

Thermal analysis

TG (a), DTA (b) and DTG (c) curves of CoHPM and 20CoHPM/Tween60 composite are presented in Fig. 7. Earlier research has shown that during the thermal treatment of molybdophosphoric acid, two main endothermic processes are observed: the loss of crystallization and/or adsorbed water (forming anhydrous heteropolyoxo compound) and the formation of constitution water (which originates from acidic protons and the oxygen belonging to the Keggin anion). At high temperature, there is the structural transformation (destruction) of Keggin anion accompanied by exothermic effect [37, 38].

The DTA curve of hydrated CoHPM shows that formation of anhydrous species progresses in several steps. Namely, four endothermic peaks, two large at 343 and 516 K and two shoulders at 358 and 398 K, could be observed. Small peak at 573 K corresponds to endothermal formation of constitutional water from acid proton and oxygen from Keggin anion. The final process is evidenced by an exothermic peak at 733 K assigned to slow solid-state transformation to molybdenum oxide and another at 890 K which can be assigned to the crystallization of the oxides resulting from the total decomposition of the Keggin units.

A different thermal behaviour is observed after supporting CoHPMo on mesoporous silica with Tween 60. The endothermic effect at 351 K is due to the additive thermal effects of the desorbed water from mesoporous silica surface and to the loss of the first part of the CoHPM crystallization water. A second endothermal process which

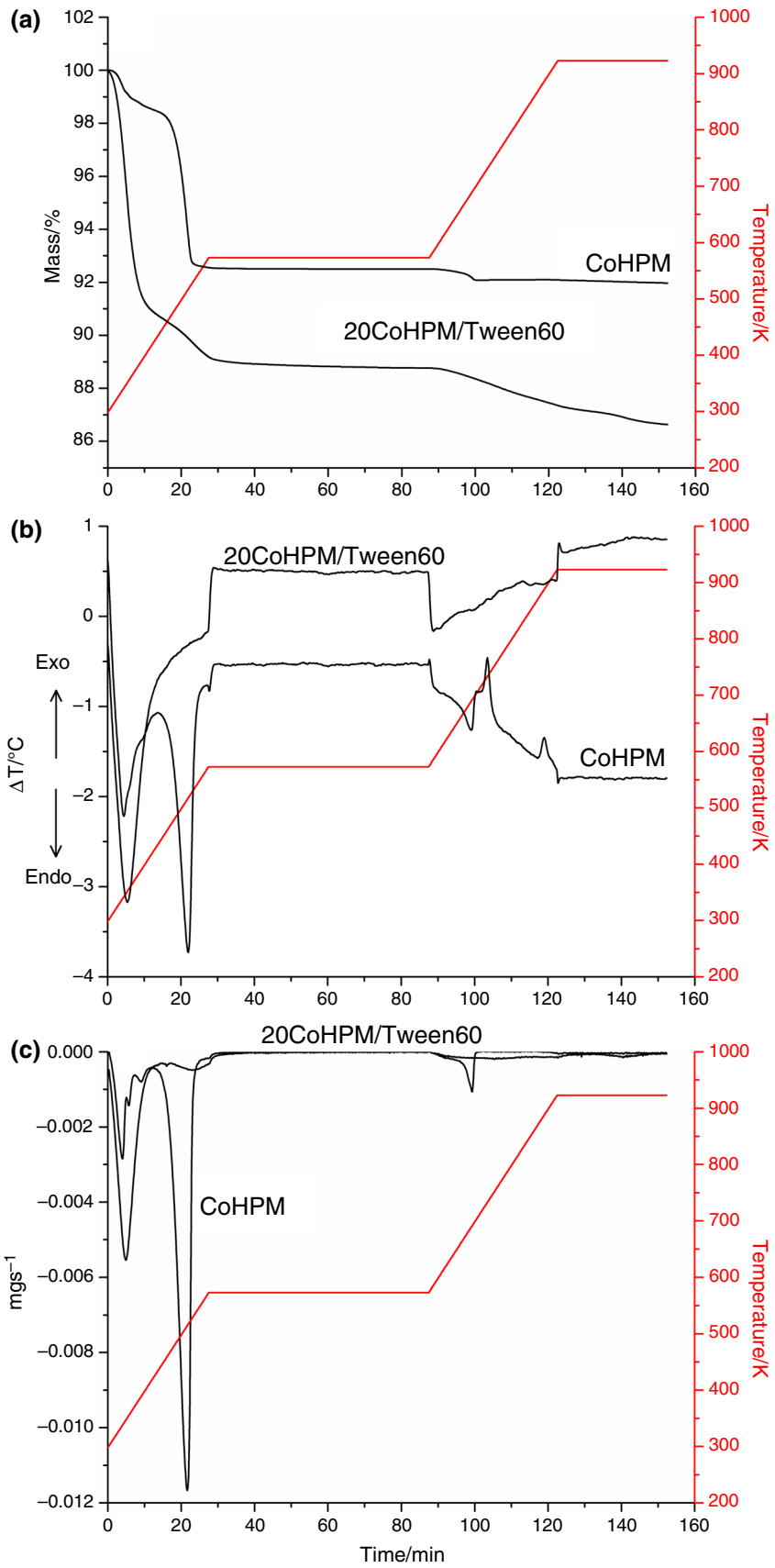

Fig. 7 Thermal analysis curves of CoHPM and 20CoHPM/Tween60 composite: TG (**a**), DTA (**b**) and DTG (**c**)

appears at 546 K is due to the loss of the second part of the crystallization water (Fig. 7a–c). The loss of the crystallization water is completed at 573 K after 1/2 h of isothermal treatment at this temperature. In the temperature range 573–923 K a slow and continuous loss of sample mass is proceeding, owing to the release of constitutive water molecules of the CoHPM and of the OH^- groups of mesoporous silica. Due to the porous morphology of mesoporous silica, all the processes of water release for CoHPM/Tween 60 composites are continual without intense peaks on DTA curves.

The exothermic peak could not be observed until 923 K on the DTA curve of all composites (only data for 20CoHPM/Tween 60 are presented). *Therefore, CoHPM/Tween 60 composites exhibit higher thermal stability then bulk CoHPM salt*.

For a better visualization of thermal effects of pure Co salts and CoHPM/Tween 60 composites, DSC method was used (Fig. 8). As on the DTA curve, in the low temperature region of DSC curve of pure CoHPM are observed two endothermic peaks at 355 and 501 K assigned to formation of anhydrous species by elimination of desorbed and crystallization water.

Three exothermic effects are observed for pure CoHPM at 699, 735 and 896 K on DSC curve (Fig. 8). As was described for DTA curve, the exothermic effects are assigned to the crystallization of constitutive oxides. *Only two distinct exothermic peaks, at higher temperatures than at DSC curve, could be observed on DTA curve*.

In a previous paper, we studied the DSC analysis of $NiHPMo_{12}O_{40}$ supported on SBA-15 [39]. The assignment of DSC peaks for CoHPM/Tween 60 composites was done according to our previous paper and to some of references contained in that paper. Therefore, on DSC curve the exothermic peak at 699 K might be assign to the crystallization of β-MoO_3. Maksimovskaya et al. [40] reported that near 673 K $HPMo_{12}O_{39}$ transforms into MoO_2HPO_4 and MoO_3 or $[PMo_{12}O_{38}][PMo_{12}O_{39}]$ (the so-called anhydride 2). Above 723 K anhydride 2 decomposes to yield $(MoO_2)_2(P_2O_7)$ and α-MoO_3, corresponding to the exothermic peak at 735 K. The exothermic peak at 896 K is due to the crystallization of the resulting α-MoO_3.

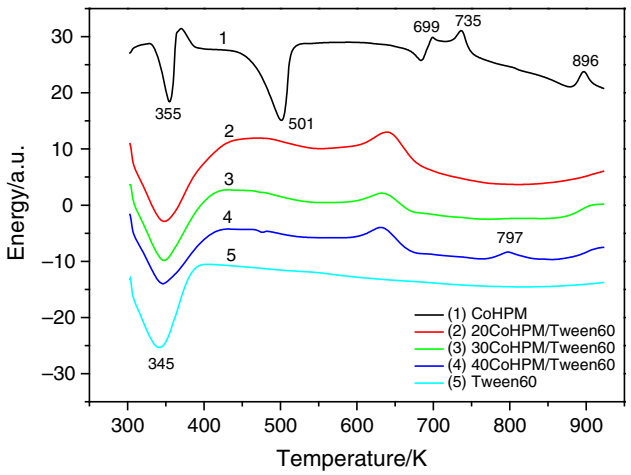

Fig. 8 DSC analysis of CoHPM/Tween 60 composites

For 40CoHPM/Tween 60 composites is observed an exothermic peak on DSC curve at 797 K which is the corresponding peak from 735 K of pure CoHPM. So it could be supposed that the decomposition process of anhydride 2 to yield $(MoO_2)_2(P_2O_7)$ and α-MoO_3 is delayed in the case of supported CoHPM. For all CoHPM/Tween 60 composites is observed above 723 K the beginning of an exothermic process with the maximum at around 923 K. This peak is the corresponding peak from 896 K of pure CoHPM which is due to the crystallization of the resulting α-MoO_3. We cannot see the whole peak at 923 K because the analysis should stop at this temperature in order to avoid the vaporization of molybdenum.

Therefore, immobilization on mesoporous silica with Tween 60 obviously increases the thermal stability of the Keggin structure in comparison with its parent bulk CoHPM, probably due to the interaction of active phase with surface silanols on the support.

Conclusions

In this study a procedure for impregnation of Keggin-type HPAs Co salt into ordered mesoporous silica obtained by using a non-ionic surfactant, Tween 60 is described. After impregnation on ordered mesoporous silica, the HPAs anions preserved their Keggin structure on the surface of mesoporous silica–HPA composites and form finely dispersed heteropolyacid species. The favourable effect of heteropolyacid impregnation on mesoporous silica is the increasing of pore volume and specific surface area in comparison with pure active phase, which enables better accessibility of catalyst active centres and renders the silica–HPA composites appropriate for heterogeneous catalysis. The mesoporous silica–HPA composites are thermally more stable than the parent acids, due to the strong anion-support interaction.

From SEM–EDS analysis, it could be observed that for low loading of active phase, the average content of elements is close to the stoichiometric one, while for higher loadings, the samples exhibit a higher deviation of Mo, P and Co concentration values from the stoichiometric ones. In the latter case, it could be supposed that active phase was less homogeneously dispersed inside the composites pores than for low loadings of active phase.

Raman and FT-IR spectroscopy confirmed that the Keggin structure is well preserved on the mesoporous silica support after its impregnation with CoHPM and that thermal treatment enabled better dispersion of the active phase in the support. These observations are in accordance with earlier findings indicating the reliability of the applied preparation method. *This information together with those acquired by PXRD, thermal analysis and SEM–EDS suggests a strong interaction between the host silica network and the guest CoHPM molecules, and a weaker interactions among the Keggin anions*. It follows that HPAs in the silica-included samples prepared here are finely dispersed and strongly bound in the porous silica network.

Therefore, immobilization on mesoporous silica with Tween 60 obviously increases the thermal stability of the Keggin structure in comparison with its parent bulk CoHPM, probably due to the interaction of active phase with surface silanols on the support.

Acknowledgements These investigations were partially financed by Romanian Academy Project No. 4.3 and by the Ministry of Education and Science of Republic of Serbia, Grants 172043.

References

1. Omwoma S, Gore CT, Ji Y, Hu C, Song Y-F. Environmentally benign polyoxometalate materials. Coord Chem Rev. 2015;286:17–29.
2. Cavani F. Heteropolycompound-based catalysts: a blend of acid and oxidizing properties. Catal Today. 1998;41:73–86.
3. Kwon HJ, Kwon SC, Seo GJ, Lee C, Jo G. US Patent 2013/026.099.0A1. 2013.
4. Jiang C, Guo Y, Wang C, Hu C, Wu Y, Wang E. Synthesis of dimethyl carbonate from methanol and carbon dioxide in the presence of polyoxometalates under mild conditions. Appl Catal A. 2003;256:203–12.
5. Yan X-M, Lei J-H, Liu D, Wu Y-C, Liu W. Synthesis and catalytic properties of mesoporous phosphotungstic acid/SiO_2 in a self-generated acidic environment by evaporation-induced self-assembly. Mater Res Bull. 2007;42:1905–13.
6. Khalameida SV, Sydorchuk VV, Skubiszewska-Zięba J, Leboda R, Zazhigalov VA. Sol–gel synthesis and properties of compositions containing heteropoly compounds in porous silica matrix. Glass Phys Chem. 2014;40(1):8–16.
7. Popa A, Sasca V, Kis EE, Marinkovic-Neducin R, Holclajtner-Antunović I. Mesoporous silica directly modified by incorporation or impregnation of some hetyeropolyacids: synthesis and structural characterization. Mater Res Bull. 2011;46:19–25.
8. Shen L, Feng Y, Yin H, Wang A, Yu L, Jiang T, Shen Y, Wu Z. Gas phase dehydration of glycerol catalyzed by rutile TiO_2-supported heteropolyacids. J Ind Eng Chem. 2011;17:484–92.
9. Rao PSN, Parameswaram G, Rao AVP, Lingaiah N. Influence of cesium and vanadium contents on the oxidation functionalities of heteropoly molybdate catalysts. J Mol Catal A: Chem. 2015;399:62–70.
10. Long X, Wang Z, Wu S, Wu Sh, Lv H, Yuan W. Production of isophthalic acid from m-xylene oxidation under the catalysis of the $H_3PW_{12}O_{40}$/carbon and cobalt catalytic system. J Ind Eng Chem. 2014;20(1):100–7.
11. Ferreira P, Fonseca IM, Ramos AM, Vital J, Castanheiro JE. Acetylation of glycerol over heteropolyacids supported on activated carbon. Catal Commun. 2011;12:573–6.
12. Jing F, Katryniok B, Dumeignil F, Bordes-Richard E, Paul S. Catalytic selective oxidation of isobutane to methacrylic acid on supported $(NH_4)_3HPMo_{11}VO_{40}$ catalysts. J Catal. 2014;309:121–35.
13. Holclajtner-Antunovic I, Bajuk-Bogdanovic D, Popa A, Vasiljevia BN, Krstic J, Mentus S, Uskokovic-Markovic S. Structural, morphological and catalytic characterization of neutral Ag salt of 12-tungstophosphoric acid: influence of preparation conditions. Appl Surf Sci. 2015;328:466–74.
14. Matachowski L, Drelinkiewicz A, Mucha D, Krysciak-Czerwenka J, Rachwalik R. Preparation of active $Cs_2HPW_{12}O_{40}$ catalyst with the 'core–shell' secondary structure by a self-organizing process. Appl Catal A Gen. 2014;469:239–49.
15. Hasik M, Pozniczek J, Piwowarska Z, Dziembaj R, Bielanski A, Pron A. Catalytic conversion of ethyl alcohol on polyaniline protonated with 12-tungstosilicic acid. J Mol Catal. 1994;89:329–44.
16. Popa A, Pleşu N, Sasca V, Kiš EE, Marinković-Nedučin R. Physicochemical features of polyaniline supported heteropolyacids. J Optoelectron Adv Mater. 2006;8(5):1944–50.
17. Patel A, Singh S. A green and sustainable approach for esterification of glycerol using 12-tungstophosphoric acid anchored to different supports: kinetics and effect of support. Fuel. 2014;118:358–64.
18. Costa CC, Melo DMA, Fontes MSB, Barros JMF, Melo MAF, Martinelli AE. Kinetic study of the removal of pure and mixed TTMA + , CTMA + and DTMA + templates from MCM-41. J Therm Anal Calorim. 2015;122:1485–91.
19. Khder AERS, Hassan HMA, El-Shall MS. Acid catalyzed organic transformations by heteropoly tungstophosphoric acid supported on MCM-41. Appl Catal A Gen. 2012;411–412:77–86.
20. Kim I, Kim J, Lee D. A comparative study on catalytic properties of solid acid catalysts for glycerol acetylation at low temperatures. Appl Catal B Environ. 2014;148–149:295–303.
21. Sheng X, Kong J, Zhou Y, Zhang Y, Zhang Z, Zhou S. Direct synthesis, characterization and catalytic application of SBA-15 mesoporous silica with heteropolyacid incorporated into their framework. Microporous Mesoporous Mater. 2014;187:7–13.
22. Yilmaz MS, Piskin S. The removal of template from SBA-15 samples synthesized from different silica sources. J Therm Anal Calorim. 2015;121:1255–62.
23. Jing F, Katryniok B, Bordes-Richard E, Paul S. Improvement of the catalytic performance of supported $(NH_4)_3HPMo_{11}VO_{40}$ catalysts in isobutane selective oxidation. Catal Today. 2013;203:32–9.
24. Rao PM, Landau MV, Wolfson A, Shapira-Tchelet AM, Herskowitz M. Cesium salt of a heteropolyacid in nanotubular channels and on the external surface of SBA-15 crystals: preparation and performance as acidic catalysts. Microporous Mesoporous Mater. 2005;80:43–55.
25. Nowinska K, Formaniak R, Kaleta W, Waclaw A. Heteropoly compounds incorporated into mesoporous material structure. Appl Catal A Gen. 2003;256:115–23.
26. Benadji S, Eloy P, Leonard A, Su B-L, Rabia C, Gaigneaux EM. Characterization of $H_{3+x}PMo_{12-x}V_xO_{40}$ heteropolyacids supported on HMS mesoporous molecular sieve and their catalytic performance in propene oxidation. Microporous Mesoporous Mater. 2012;154:153–63.
27. Trach Y, Sydorchuk V, Makota O, Khalameida S, Leboda R, Skubiszewska-Zieba J, Zazhigalov V. Synthesis, physical–chemical, and catalytic properties of mixed compositions Ag/$H_3PMo_{12}O_{40}$/SiO_2. J Therm Anal Calorim. 2012;107:453–61.

28. Shimizu K, Niimi K, Satsuma A. Polyvalent-metal salts of heteropolyacid as catalyst for Friedel-Crafts alkylation reactions. Appl Catal A. 2008;349:1–5.
29. Aouissi A, Al-Deyab SS, Al-Owais A, Al-Amro A. Reactivity of heteropolytungstate and heteropolymolybdate metal transition salts in the synthesis of dimethyl carbonate from methanol and CO_2. Int J Mol Sci. 2010;11:2770–9.
30. Mizuno N, Misono M. Heterogeneous catalysis. Chem Rev. 1998;98:199–217.
31. Ono Y. Heteropoly acids catalysis – a unique blend of acid-base and redox properties. In: Thomas JM, Zamaraev KI, editors. Perspectives in catalysis. London: Blackwell; 1992. pp 431–63.
32. Toufaily J, Soulard M, Guth J-L, Patarin J, Delmonte L, Hamieh T, Kodeih M, Naoufal D, Hamad H. Synthesis and characterization of new catalysts formed by direct incorporation of heteropolyacids into organized mesoporous silica. Colloids Surf. 2008;316:285–91.
33. Rocchiccioli-Deltcheff C, Fournier M, Frank R, Thouvenot R. Vibrational investigations of polyoxometalates. 2. Evidence for anion-anion interactions in molybdenum (VI) and tungsten (VI) compounds related to the Keggin structure. Inorg Chem. 1983;22:207–16.
34. Bridgeman AJ. Density functional study of the vibrational frequencies of α-Keggin heteropolyanions. Chem Phys. 2003;287:55–69.
35. Rocchiccioli-Deltcheff C, Amirouche M, Fournier M, Frank R. Structure and catalytic properties of silica-supported polyoxomolybdates III. 12-molybdosilicic acid catalysts: vibrational study of the dispersion effect and nature of the Mo species in interaction with the silica support. J Catal. 1992;138:445–56.
36. Guo Y, Li K, Yu X, Clark JH. Mesoporous $H_3PW_{12}O_{40}$-silica composite: efficient and reusable solid acid catalyst for the synthesis of diphenolic acid from levulinic acid. Appl Catal B Environ. 2008;81:182–91.
37. Sasca V, Stefanescu M, Popa A. Studies on the Non-Isothermal Decomposition of $H_3PMo_{12}O_{40}{\cdot}xH_2O$ and $H_4PVMo_{11}O_{40}{\cdot}yH_2O$. J Therm Anal Calorim. 1999;56:569–78.
38. Popa A, Sasca V, Stefănescu M, Kis EE, Marinkovic-Neducin R. The influence of the nature and textural properties of different supports on the thermal behavior of Keggin type heteropolyacids. J Serb Chem Soc. 2006;71(3):235–49.
39. Popa A, Sasca V, Bajuk-Bogdanović D, Holclajtner-Antunović I. Acidic nickel salts of Keggin type heteropolyacids supported on SBA-15 mesoporous silica. J Porous Mater. 2016;23(1):211–23.
40. Maksimovskaya RI, Maksimov GM, Litvak GS. Thermal transformations of α-$H_6P_2Mo_{18}O_{62}{\cdot}nH_2O$ heteropolyacid. Russ J Chem Bull Int Ed. 2003;52:103–8.